Electrochemistry Communications 140 (2022) 107340

Contents lists available at ScienceDirect

Electrochemistry Communications

journal homepage: www.elsevier.com/locate/elecom

Effect of proton conductivity transients on PEM fuel cell impedance: Formation of a low–frequency inductive loop

Andrei Kulikovsky [1,2]

Forschungszentrum Jülich GmbH, Theory and Computation of Energy Materials (IEK-13), Institute of Energy and Climate Research, D–52425 Jülich, Germany

ARTICLE INFO

Keywords:
PEM fuel cell
Impedance
Proton conductivity
Modeling

ABSTRACT

A model for PEMFC cathode impedance is developed. The model includes transient response of catalyst layer proton conductivity to cell current density variation. Analytical solution shows that transient conductivity leads to formation of a low–frequency inductive loop in the Nyquist spectrum. This loop has been observed in numerous experiments and its nature has long been discussed in literature. The results of this work provide a new mechanism of loop formation.

1. Introduction

Liquid water is one of the key ingredients for PEM fuel cell operation as polymer electrolyte membrane separating anode and cathode conducts protons only in hydrated state. Amount of water produced in the oxygen reduction reaction (ORR) on the cathode side is usually insufficient to provide fully hydrated state of the membrane and external humidification of hydrogen and air streams is necessary.

This leads to quite complicated problem of water transport and transformation in the cell. Water vapor added to the hydrogen flux is transported through the membrane with proton current by electroosmotic drag, while water produced on the cathode side is transported to the anode by back diffusion. Inside the membrane, water exists in liquid state due to huge pressure provided by electric fields of separated charges [1]; membrane surface performs "phase transformation" of water vapor to liquid according to water sorption isotherm [2].

The membrane water content is usually expressed as a number of water molecules λ_s per sulphonic group. Springer, Zawodzinski and Gottesfeld [3] measured water diffusion D_w and drag n_d coefficients and showed that D_w and n_d depend on λ_s. This makes the problem of water transport through the cell sandwich nonlinear.

In Nafion membranes, a linear dependence of membrane proton conductivity σ_m on λ_s at the cell temperature of 273 +30 K has been reported [3]:

$$\sigma_m = \begin{cases} 0.005139\lambda_s - 0.00326, & \lambda_s > 1, \\ 0.005139 & \lambda_s \leqslant 1 \end{cases} \quad \text{S cm}^{-1} \tag{1}$$

The Arrhenius temperature factor for σ_m has also been given in [3].

Proton transport in the cathode catalyst layer (CCL) is provided by a cluster of membrane phase. Much like in the bulk membrane, water transport in the membrane phase is due to electroosmotic drag and diffusion. The mechanism of interfacial water transformation at the ionomer/pore interface inside the CCL is not well understood. The proton conductivity of CCL σ is usually calculated by multiplying Eq. (1) by the Bruggeman correction factor $\epsilon^{1.5}$, where ϵ is the volume fraction of Nafion in the CCL [4]:

$$\sigma = \epsilon^{1.5}\sigma_m \tag{2}$$

Not surprisingly, CCL proton conductivity in operating PEMFC depends on the cell current density j. Impedance spectroscopy shows almost linear growth of σ with j (Fig. 1). This growth can be attributed to growing with the current liquid water content of the CCL, translating the linear growth of σ with λ_s, Eq. (1), into the linear growth of σ with j.

From this discussion it follows that the response of σ on the change in cell current is not immediate: some relaxation time τ_s determined by water drag, diffusion and sorption/desorption is needed for σ to reach a new steady state. In this work, a model for the CCL impedance taking into account transients of proton conductivity is developed. In the case of fast oxygen transport, analytical solution for the CCL impedance is derived. The Nyquist spectrum exhibits a low–frequency (LF) inductive loop representing impedance due to variable proton conductivity with time.

E-mail address: A.Kulikovsky@fz-juelich.de.
[1] ISE member
[2] Lomonosov Moscow State University, Research Computing Center, 119991 Moscow, Russia.

https://doi.org/10.1016/j.elecom.2022.107340
Received 18 July 2022; Received in revised form 30 July 2022; Accepted 2 August 2022
Available online 5 August 2022

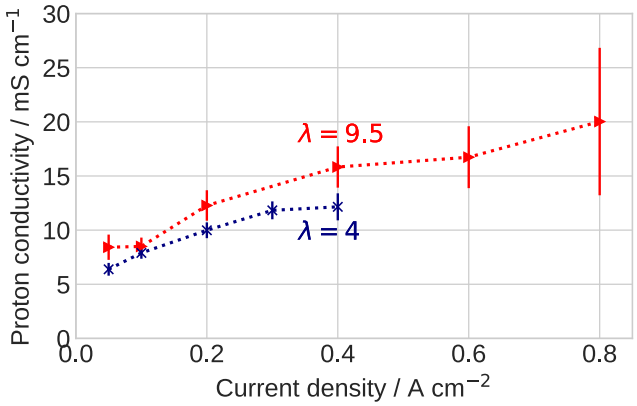

Fig. 1. CCL proton conductivity vs cell current density in operating Pt/C–based PEMFC for the indicated stoichiometry λ of the air flow. The data have been obtained by fitting the impedance model (Ref. [5], Chapter 6) to experimental impedance spectra. The spectra have been measured at the cell temperature of 80°C, pressure at the anode/cathode of 150/150 kPa, relative humidity 100/50%. The other experimental details can be found in [6].

2. Model

2.1. Equation for the conductivity variation with time

Fig. 1 shows that the CCL proton conductivity increases with the cell current density from $\sigma_* \simeq 5$ mS cm^{-1} at small currents up to $\simeq$ 15–20 mS cm^{-1} at higher currents. For simplicity, we will assume that the growth of σ with j up to 1 A cm^{-2} is linear

$$\sigma^0(j) = \sigma_*(1+\beta j), \quad 0 \leqslant j \leqslant 1 \quad \text{A cm}^{-2} \tag{3}$$

where $\sigma_* \simeq 5$ mS cm^{-1} is the conductivity at zero current, and β determines the slope of the straight line.

As discussed above, we will assume that some relaxation time τ_s is necessary to establish equilibrium between the water flux and membrane phase water content in the CCL. A simplest model equation for variation of conductivity with time is

$$\tau_s \frac{\partial \sigma}{\partial t} + \sigma = \sigma^0 \tag{4}$$

Eq. (4) describes exponential approach of proton conductivity to its stationary shape σ^0 with τ_s being the characteristic time of σ growth.

It is convenient to introduce dimensionless variables

$$\widetilde{t} = \frac{t}{t_*}, \quad \widetilde{x} = \frac{x}{l_t}, \quad \widetilde{\sigma} = \frac{\sigma}{\sigma_*}, \quad \widetilde{j} = \frac{j}{j_*}, \quad \widetilde{\eta} = \frac{\eta}{b}, \quad \widetilde{\omega} = \omega t_*, \quad \widetilde{Z} = \frac{Z\sigma_*}{l_t} \tag{5}$$

where l_t is the CCL thickness, b is the ORR Tafel slope, Z is the impedance, ω is the angular frequency of the AC signal, and the time t_* and current density j_* scales are given by

$$t_* = \frac{C_{dl} b}{i_*}, \quad j_* = \frac{\sigma_* b}{l_t} \tag{6}$$

Here, C_{dl} is the double layer capacitance and i_* is the ORR volumetric exchange current density.

With Eqs. (5), Eq. (4) transforms to

$$\mu_s^2 \frac{\partial \widetilde{\sigma}}{\partial \widetilde{t}} + \widetilde{\sigma} = \widetilde{\sigma}^0\left(\widetilde{j}\right). \tag{7}$$

Here,

$$\widetilde{\sigma}^0 = 1 + \widetilde{\beta}\widetilde{j}, \quad \widetilde{\beta} \equiv \beta j_* \tag{8}$$

and

$$\mu_s = \sqrt{\frac{\tau_s i_*}{C_{dl} b}}. \tag{9}$$

To perform linearization and Fourier–transform, we substitute the following expansions into Eq. (4)

$$\begin{aligned} \widetilde{\sigma} &= \widetilde{\sigma}^0 + \widetilde{\sigma}^1(\widetilde{\omega})\exp(\mathrm{i}\widetilde{\omega}\widetilde{t}), \quad \widetilde{\sigma}^1 \ll \widetilde{\sigma}^0 \\ \widetilde{j} &= \widetilde{j}^0 + \widetilde{j}^1(\widetilde{\omega})\exp(\mathrm{i}\widetilde{\omega}\widetilde{t}), \quad \widetilde{j}^1 \ll \widetilde{j}^0, \end{aligned} \tag{10}$$

and subtract the static equation from the result. This leads to the linear algebraic equation for the perturbation amplitude $\widetilde{\sigma}^1$:

$$\mathrm{i}\widetilde{\omega}\mu_s^2\widetilde{\sigma}^1 + \widetilde{\sigma}^1 = \frac{\partial \widetilde{\sigma}^0}{\partial \widetilde{j}}\widetilde{j}^1. \tag{11}$$

Here and below, the superscripts 0 and 1 mark the static variables and the AC perturbation amplitudes in the $\widetilde{\omega}$–space, respectively.

Calculating the derivative $\partial\widetilde{\sigma}^0/\partial\widetilde{j}$ with Eq. (8), from Eq. (11) we get

$$\widetilde{\sigma}^1 = k_s\widetilde{j}^1, \quad k_s = \frac{\widetilde{\beta}}{1+\mathrm{i}\widetilde{\omega}\mu_s^2}. \tag{12}$$

For further references we need to relate $\widetilde{j}^1$ with $\partial\widetilde{\eta}^1/\partial\widetilde{x}$. From the Ohm's law we have

$$\widetilde{j}^0 + \widetilde{j}^1 = -\left(\widetilde{\sigma}^0 + \widetilde{\sigma}^1\right)\frac{\partial(\widetilde{\eta}^0 + \widetilde{\eta}^1)}{\partial\widetilde{x}} \tag{13}$$

Subtracting from this equation the static Ohm's law $\widetilde{j}^0 = -\widetilde{\sigma}^0\partial\widetilde{\eta}^0/\partial\widetilde{x}$ and neglecting the small term $\widetilde{\sigma}^1\partial\widetilde{\eta}^1/\partial\widetilde{x}$, we get

$$\widetilde{j}^1 = -\widetilde{\sigma}^0\frac{\partial\widetilde{\eta}^1}{\partial\widetilde{x}} - \widetilde{\sigma}^1\frac{\partial\widetilde{\eta}^0}{\partial\widetilde{x}} = -\widetilde{\sigma}^0\frac{\partial\widetilde{\eta}^1}{\partial\widetilde{x}} + \frac{\widetilde{\sigma}^1}{\widetilde{\sigma}^0}\widetilde{j}^0 \tag{14}$$

Using here Eq. (12) in the last term, we get equation for $\widetilde{j}^1$, which leads to

$$\widetilde{j}^1 = -\left(\frac{\widetilde{\sigma}^0}{1 - k_s\widetilde{j}^0/\widetilde{\sigma}^0}\right)\frac{\partial\widetilde{\eta}^1}{\partial\widetilde{x}}. \tag{15}$$

With Eq. (15), Eq. (12) takes the form

$$\widetilde{\sigma}^1 = -\left(\frac{k_s\widetilde{\sigma}^0}{1 - k_s\widetilde{j}^0/\widetilde{\sigma}^0}\right)\frac{\partial\widetilde{\eta}^1}{\partial\widetilde{x}} \tag{16}$$

2.2. Equation for the overpotential perturbation

With the time–dependent σ, the dimensionless equation for ORR overpotential [7] transforms to

$$\frac{\partial\widetilde{\eta}}{\partial\widetilde{t}} - \varepsilon^2\widetilde{\sigma}\frac{\partial^2\widetilde{\eta}}{\partial\widetilde{x}^2} = -\widetilde{c}\exp\widetilde{\eta} \tag{17}$$

where

$$\varepsilon = \sqrt{\frac{\sigma_* b}{i_* l_t^2}} \tag{18}$$

Obviously, the static equation for $\widetilde{\eta}^0$ reads

$$\varepsilon^2\widetilde{\sigma}^0\frac{\partial^2\widetilde{\eta}^0}{\partial\widetilde{x}^2} = \widetilde{c}^0\exp\widetilde{\eta}^0 \tag{19}$$

Substitution of

$$\begin{aligned}\widetilde{\sigma} &= \widetilde{\sigma}^0 + \widetilde{\sigma}^1(\widetilde{\omega})\exp(\mathrm{i}\widetilde{\omega}\widetilde{t}), \quad \widetilde{\sigma}^1 \ll \widetilde{\sigma}^0 \\ \widetilde{\eta} &= \widetilde{\eta}^0(\widetilde{x}) + \widetilde{\eta}^1(\widetilde{x},\widetilde{\omega})\exp(\mathrm{i}\widetilde{\omega}\widetilde{t}), \quad \widetilde{\eta}^1 \ll \widetilde{\eta}^0,\end{aligned} \tag{20}$$

into Eq. (17), performing linearization of the right side and subtracting Eq. (19), we come to

$$\varepsilon^2\widetilde{\sigma}^0\frac{\partial^2\widetilde{\eta}^1}{\partial\widetilde{x}^2} + \varepsilon^2\widetilde{\sigma}^1\frac{\partial^2\widetilde{\eta}^0}{\partial\widetilde{x}^2} = \mathrm{e}^{\widetilde{\eta}^0}\widetilde{c}^1 + \left(\widetilde{c}^0\mathrm{e}^{\widetilde{\eta}^0} + \mathrm{i}\widetilde{\omega}\right)\widetilde{\eta}^1 \tag{21}$$

Using Eq. (19) to eliminate $\partial^2\widetilde{\eta}^0/\partial\widetilde{x}^2$, Eq. (21) transforms to

$$\varepsilon^2\widetilde{\sigma}^0\frac{\partial^2\widetilde{\eta}^1}{\partial\widetilde{x}^2} + \frac{\widetilde{\sigma}^1}{\widetilde{\sigma}^0}\widetilde{c}^0\exp\widetilde{\eta}^0 = \mathrm{e}^{\widetilde{\eta}^0}\widetilde{c}^1 + \left(\widetilde{c}^0\mathrm{e}^{\widetilde{\eta}^0} + \mathrm{i}\widetilde{\omega}\right)\widetilde{\eta}^1 \tag{22}$$

Taking into account Eq. (16), we arrive at

$$\varepsilon^2\widetilde{\sigma}^0\frac{\partial^2\widetilde{\eta}^1}{\partial\widetilde{x}^2} - \left(\frac{k_x\widetilde{c}^0\exp\widetilde{\eta}^0}{1 - k_x\widetilde{j}^0/\widetilde{\sigma}^0}\right)\frac{\partial\widetilde{\eta}^1}{\partial\widetilde{x}} = \mathrm{e}^{\widetilde{\eta}^0}\widetilde{c}^1 + \left(\widetilde{c}^0\mathrm{e}^{\widetilde{\eta}^0} + \mathrm{i}\widetilde{\omega}\right)\widetilde{\eta}^1 \tag{23}$$

Eq. (23) is the general equation for the ORR overpotential perturbation with the account of proton conductivity transients.

2.3. Fast oxygen transport: Impedance

Consider for simplicity a low–current regime of cell operation. In that case, variation of $\widetilde{\eta}^0$ with $\widetilde{x}$ is small and using the Tafel equation $\varepsilon^2\widetilde{j}^0 = \widetilde{c}^0\exp\widetilde{\eta}^0$, Eq. (22) further reduces to

$$\varepsilon^2\widetilde{\sigma}^0\frac{\partial^2\widetilde{\eta}^1}{\partial\widetilde{x}^2} - \left(\frac{\varepsilon^2 k_x\widetilde{j}^0}{1 - k_x\widetilde{j}^0/\widetilde{\sigma}^0}\right)\frac{\partial\widetilde{\eta}^1}{\partial\widetilde{x}} = \mathrm{e}^{\widetilde{\eta}^0}\widetilde{c}^1 + \left(\varepsilon^2\widetilde{j}^0 + \mathrm{i}\widetilde{\omega}\right)\widetilde{\eta}^1 \tag{24}$$

It is advisable to consider the case of fast oxygen transport in the CCL. In this regime, we may set $\widetilde{c}^1 = 0$, and Eq. (24) simplifies to

$$\widetilde{\sigma}^0\frac{\partial^2\widetilde{\eta}^1}{\partial\widetilde{x}^2} - \phi_1\frac{\partial\widetilde{\eta}^1}{\partial\widetilde{x}} = \alpha\widetilde{\eta}^1, \quad \widetilde{\eta}^1(1) = \widetilde{\eta}^1_1, \quad \left.\frac{\partial\widetilde{\eta}^1}{\partial\widetilde{x}}\right|_{\widetilde{x}=1} = 0, \tag{25}$$

where

$$\alpha = \widetilde{j}^0 + \frac{\mathrm{i}\widetilde{\omega}}{\varepsilon^2}, \quad \phi_1 = \frac{k_x\widetilde{j}^0}{1 - k_x\widetilde{j}^0/\widetilde{\sigma}^0} \tag{26}$$

and the boundary conditions at the CCL/GDL interface ($\widetilde{x} = 1$) mean applied perturbation $\widetilde{\eta}^1_1$ and zero proton current.

Solving Eq. (25) and calculating the CCL impedance $\widetilde{Z}$ according to

$$\widetilde{Z} = \left.\frac{\widetilde{\eta}^1}{\widetilde{j}^1}\right|_{\widetilde{x}=0} \tag{27}$$

where $\widetilde{j}^1$ is given by Eq. (15), we get

$$\widetilde{Z} = \frac{\left(1 - k_x\widetilde{j}^0/\widetilde{\sigma}^0\right)\sqrt{4\alpha\widetilde{\sigma}^0 + \phi_1^2}}{2\alpha\widetilde{\sigma}^0\tanh\left(\sqrt{4\alpha\widetilde{\sigma}^0 + \phi_1^2}\Big/\left(2\widetilde{\sigma}^0\right)\right)} + \frac{k_x\widetilde{j}^0}{2\alpha\widetilde{\sigma}^0} \tag{28}$$

3. Results and discussion

The spectra of impedance Eq. (28) for the typical cell parameters in Table 1 and the relaxation time $\tau_s = 10$ s are shown in Fig. 2. As can be seen, transient variation of σ with the cell current density leads to formation of the LF loop in the Nyquist spectra. The characteristic frequency of this loop is $f_s = 1/(2\pi\tau_s)$ (Fig. 2b). Upon variation of τ_s in the range of 0.1 to 100 s, the loop amplitude decreases with the decrease in τ_s.

Table 1
The cell parameters used in calculations.

CCL thickness l_t, cm	$10{\cdot}10^{-4}$
Proton conductivity σ_*, S cm^{-1}	$5{\cdot}10^{-3}$
Parameter β in Eq. (3), $^{-1}$ cm^2	1
ORR Tafel slope b, V/ exp	0.03
Double layer capacitance C_{dl}, F cm^{-3}	20
Cell current density j^0, A cm^{-2}	0.1
Pressure	Standard
Cell temperature T, K	273 + 80

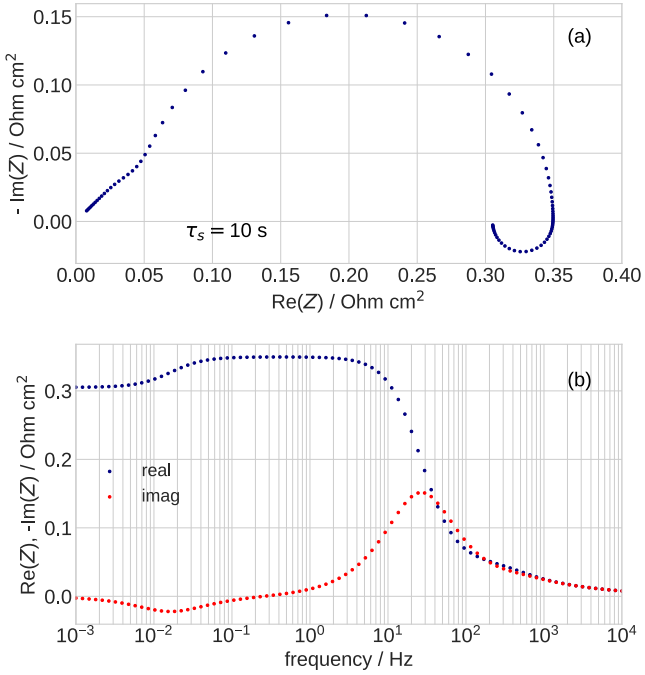

Fig. 2. (a) The Nyquist spectrum of Eq. (28) for the proton conductivity relaxation time $\tau_s = 10$ s. The other parameters are listed in Table 1. (b) The frequency dependence of the real and imaginary parts of the impedance in (a).

Calculation of limit $\widetilde{Z}$, Eq. (28), as $\widetilde{\omega}\to 0$ and further Taylor series expansion at small $\widetilde{j}^0$ leads to the static resistivity of the CCL. At leading order, R_{CCL} in the dimension form reads

$$R_{CCL} = \frac{l_t}{3\sigma} + \frac{b}{j^0} - \frac{\beta b}{2} \tag{29}$$

Note that β has a dimension of inverse current density. The first term on the right side of Eq. (29) gives the resistivity of proton transport in the CCL, the second term represents the faradaic resistivity, and the third term gives the contribution of proton conductivity transients discussed above. Note that this contribution is negative, i.e., time dependence of σ reduces the differential cell resistivity.

The inductive LF loop in experimental PEMFC spectra has long been discussed in literature. Following Antoine, Bultel and Durand [8], Makharia, Mathias and Baker [9] attributed LF loop to formation of intermediates in the ORR mechanism. Roy and Orazem [10] and Roy, Orazem and Tribollet [11] attributed the loop to side reactions in PEMFC, like formation of hydrogen peroxide or Pt dissolution. Setzler and Fuller [12] developed a physics–based model with the account of Pt oxidation and showed that the model qualitatively correct predicts formation of LF loop. Wagner and Schülze [13] reported the inductive loop formation upon CO poisoning of the PEMFC cathode. Pivac and Barbir [14] provided a detailed literature review of the effect and developed equivalent circuits for LF loop description. Recently, Meyer

and Zhao [15] have shown that the LF loop forms due to variation of flow velocity by modern flow controllers in the EIS experiments with constant air flow stoichiometry. Schneider et al. [16] reported loop formation due to insufficient membrane humidification.

The model above provides yet another explanation of this effect. It should be noted that the real experimental loop may arise due to overlap of several aforementioned processes. The model above leads to the LF loop diameter proportional to β, the slope of conductivity growth with the cell current density. This dependence gives the hint for experimental verification of the loop nature: varying external humidification it could be possible to organize different slopes β in Eq. (4). Comparison of LF loop diameters could verify the mechanism above.

The assumptions of small variation of ORR overpotential through the CCL depth and of fast oxygen transport in the CCL hold if the cell current density is sufficiently small. For typical PEMFCs, the current density should be below 100 mA cm^{-2}. These assumptions are made above to derive analytical expression for the impedance, which helps to clarify the LF loop features (the characteristic frequency, and contribution to the cell resistivity). Transient CCL conductivity can, of course, be incorporated into the numerical impedance model. Preliminary results show successful fitting of measured high–current impedance spectra with LF loops. These results will be published elsewhere.

Declaration of Competing Interest

The authors declare that they have no known competing financial interests or personal relationships that could have appeared to influence the work reported in this paper.

References

[1] P. Berg, K. Ladipo, Exact solution of an electro-osmotic flow problem in a cylindrical channel of polymer electrolyte membranes, Proc. R. Soc. A 465 (2009) 2663–2679, https://doi.org/10.1098/rspa.2009.0067.
[2] M.H. Eikerling, P. Berg, Poroelectroelastic theory of water sorption and swelling in polymer electrolyte membranes, Soft Matter 7 (2011) 5976, https://doi.org/10.1039/c1sm05273j.
[3] T.E. Springer, T.A. Zawodzinski, S. Gottesfeld, Polymer electrolyte fuel cell model, J. Electrochem. Soc. 138 (8) (1991) 2334–2342.
[4] J. Dujc, A. Forner-Cuenca, P. Marmet, M. Cochet, R. Vetter, J.O. Schumacher, P. Boillat, Modeling the effects of using gas diffusion layers with patterned wettability for advanced water management in proton exchange membrane fuel cells, J. Electrochem. En. Conv. Stor. 15 (2018) 021001, https://doi.org/10.1115/1.4038626.
[5] A. Kulikovsky, Analytical Models for PEM Fuel Cell Impedance, Self–publishing, Eisma, 2022. https://www.amazon.com/Andrei-Kulikovsky/e/B00KBW7KVY.
[6] T. Reshetenko, A. Kulikovsky, PEM fuel cell characterization by means of the physical model for impedance spectra, J. Electrochem. Soc. 162 (2015) F627–F633, https://doi.org/10.1149/2.1141506jes.
[7] A. Kulikovsky, O. Shamardina, A model for PEM fuel cell impedance: Oxygen flow in the channel triggers spatial and frequency oscillations of the local impedance, J. Electrochem. Soc. 162 (2015) F1068–F1077, https://doi.org/10.1149/2.0911509jes.
[8] O. Antoine, Y. Bultel, R. Durand, Oxygen reduction reaction kinetics and mechanism on platinum nanoparticles inside Nafion, J. Electroanal. Chem. 499 (2001) 85–94, https://doi.org/10.1016/S0022-0728(00)00492-7.
[9] R. Makharia, M.F. Mathias, D.R. Baker, Measurement of catalyst layer electrolyte resistance in PEFCs using electrochemical impedance spectroscopy, J. Electrochem. Soc. 152 (2005) A970–A977, https://doi.org/10.1149/1.1888367.
[10] S.K. Roy, M.E. Orazem, Deterministic impedance models for interpretation of low frequency inductive loops in PEM fuel cells, ECS Trans. 3 (2006) 1031–1040, https://doi.org/10.1149/1.2356222.
[11] S.K. Roy, M.E. Orazem, B. Tribollet, Interpretation of low-frequency inductive loops in pem fuel cells, J. Electrochem. Soc. 154 (2007) B1378–B1388, https://doi.org/10.1149/1.2789377.
[12] B.P. Setzler, T.F. Fuller, A physics–based impedance model of proton exchange membrane fuel cells exhibiting low–frequency inductive loops, J. Electrochem. Soc. 162 (2015) F519–F530, https://doi.org/10.1149/2.0361506jes.
[13] N. Wagner, E. Gülzow, Change of electrochemical impedance spectra (EIS) with time during CO–poisoning of the Pt-anode in a membrane fuel cell, J. Power Sources 127 (2004) 341–347, https://doi.org/10.1016/j.jpowsour.2003.09.031.
[14] I. Pivac, F. Barbir, Inductive phenomena at low frequencies in impedance spectra of proton exchange membrane fuel cells – A review, J. Power Sources 326 (2016) 112–119, https://doi.org/10.1016/j.jpowsour.2016.06.119.
[15] Q. Meyer, C. Zhao, Air perturbation-induced low-frequency inductive electrochemical impedance arc in proton exchange membrane fuel cells, J. Power Sources 488 (2021) 229245, https://doi.org/10.1016/j.jpowsour.2020.229245.
[16] Schneider, et al., Impedance response of the proton exchange membrane in polymer electrolyte fuel cells, J. Electrochem. Soc. 155 (8) (2008) B783–B792, https://doi.org/10.1149/1.2929823.